## CONFERENCE PRE-PRINT

# A THRESHOLD OF MAGNETIC PERTURBATION DRIVEN BY PEELING-BALLOONING MODE AS THE MECHANISM TO TRIGGER EDGE LOCALIZED MODE CRASH

W. J. Chen<sup>1</sup>, L. W. Yan<sup>1</sup>, Y. Q. Liu<sup>2</sup>, Z. W. Ma<sup>3</sup>, D. L. Yu<sup>1</sup>, G. Z. Hao<sup>1</sup>, W. Zhang<sup>3</sup>, N. Wu<sup>1</sup>, L. Liu<sup>1</sup>, X. X. He<sup>1</sup>, Y. L. Wei<sup>1</sup>, S. Q. Wang<sup>1</sup>, S. S. Yang<sup>1</sup>, Z. B. Shi<sup>1</sup>, W. Chen<sup>1</sup>, X. Q. Ji<sup>1</sup>, and W. L. Zhong<sup>1</sup>

## **Abstract**

Edge localized mode (ELM) crash triggered by a critical threshold of magnetic perturbation with stochastic field has been investigated. Prior to the ELM crash, a clear magnetic precursor has been observed in Mirnov signal in the HL-2A tokamak, whose threshold characteristics indicates that magnetic perturbation may trigger the pedestal collapse and result in ELM crash. Nonlinear MHD simulations demonstrate that stochastic layer is generated by the magnetic reconnection process of resistivity peeling-ballooning modes. Furthermore, there is also a threshold of magnetic perturbation or sudden change of connection length, corresponding to the occurrence of the ELM crash. the simulated travelling and escaping times of test thermal particles, from the mid-plane pedestal region to the divertor plate, are consistent with the experimentally observed rise and decay times of ELM crashes.

#### 1. INTRODUCTION

The standard steady H-mode plasma is regarded as a baseline operating scenario in ITER. The good plasma confinement may result in a steep pressure and current density profiles at the edge pedestal. When the pressure gradient exceeds a certain threshold, magnetohydrodynamic (MHD) instabilities are triggered and referred to as an edge localized mode (ELM) [1]. They lead to edge pressure crash quickly and periodically. An ELM burst will transiently dump energy out into the scrape-off layer (SOL), which flows along the field lines to divertor plates and can potentially erode the divertor plate by this transient heat flux. The acceptable level of the ELM heat load is  $0.5 \text{ MJ/m}^2$  for tungsten, which is candidates for the plasma facing components of the ITER divertor[2][3][4].

This transient peak heat load depends on the type of ELMs. There are different kinds of ELMs. For example, the bursts of type-III ELMs are small and frequent. The repetition frequency decreases with heating power. The type-I ELMs have large amplitudes. The repetition frequency is typically  $10\sim100\,\mathrm{Hz}$ . As the heating power is increased, the ELMs repetition frequency also increases. The energy loss of a Type-I ELM is also much larger than that of other ELM types, being up to  $\sim20\,\%$  of the pedestal energy. Type-I and type-III ELMs are fairly universally observed. There are still other different ELM types, such as Type-II ELMs in strongly-shaped plasmas [5], grassy ELM [6][7][8], type-V ELM [9]. Understanding the physics mechanisms behind the ELM particle and energy loss from the main plasma onto the plasma-facing components is also of high interest generally.

It is widely believed that type-I ELMs are considered as periodic MHD instabilities driven by the steep current and pressure gradients at the edge transport barrier. The MHD stability codes such as ELITE have been allowed the detailed quantification of peeling-ballooning (P-B) stability boundaries and fine comparisons with observation[10]. However, the linear P-B stability boundary diagram (figure 4 in Ref. [11]) would not be sufficient to explain why the instability results in a rapid even (or burst phenomena), rather than a steady saturated mode [10]. A possible explanation for these events is explosive instabilities[12][13][14]. Although the theory for explosive instabilities in plasmas has attractive features, it does not explain all ELM events in tokamak plasmas. For example, in JET tokamak, the amplitude of instability, associated with ELM, does not grow exponentially into the ELM crash, but mostly rather linearly towards a critical value (figure 4 (d) in Ref.[15]).

There is strong evidence that at least some of these events are triggered by magnetic perturbation associated with precursor mode (see, for example, [15-20]). In the JET tokamak, C. P. Perez et al., found a low frequency (typically 5–25 kHz) coherent Type-I ELM precursor modes. The precursors are localized to a few centimeters inside the separatrix, in the pedestal region [15][16][17]. In the COMPASS-D tokamak, magnetic oscillations with frequency 70–120 kHz prior to Ohmic type I and III ELMs have been observed. And, in the example presented, the oscillations start at least 0.4 ms before the ELMs. The toroidal mode numbers were determined as

<sup>&</sup>lt;sup>1</sup> Southwestern Institute of Physics, P.O. Box 432, Chengdu, Sichuan 610041, China

<sup>&</sup>lt;sup>2</sup> General Atomics, P.O. Box 85608, San Diego, CA 92186-5608, USA

<sup>&</sup>lt;sup>3</sup> Institute for Fusion Theory and Simulation, Zhejiang University, Hangzhou, Zhejiang 310027, China Email: chenwi@swip.ac.cn

n = 4 and 5[18]. On ASDEX-Upgrade, low frequency (20 kHz) coherent oscillations starting 1 ms before ELM crash have been detected by ECE channels resonant approximately 2 cm inside the separatrix[19]. In the HL-2A tokamak, distinct precursor modes exhibiting a typical frequency of 45–50 kHz, associated with large ELM crashes, are often observed by Mirnov coils. The precursors can also be detected by the edge channels of soft X-ray cameras[20].

The ELM precursors start to grow about several hundred microseconds to several milliseconds before ELM crash. These ELM precursors are often preceded by coherent oscillations in the magnetic field. A key for investigations is whether the precursor as magnetic perturbation, derived by MHD instability, triggers the pedestal collapse and results in ELM crash. BOUT++ code simulation found that the P-B modes trigger magnetic reconnection, which leads to the pedestal collapse[21]. However, the simulation did not indicate when it would collapse. The question is whether there is a parameter that causes a phase transition during this process. Our simulation finds that there is a threshold of magnetic perturbation ( $\delta B_{\rm C}$ ) or sudden change of connection length ( $L_{\rm C}$ ), corresponding to the occurrence of the ELM crash. And the geometry of the magnetic separatrix and X-point are important. The magnetic footprints on the divertor plates are associated with the magnetic separatrix and the X-point in the presence of non-axisymmetric resonant magnetic perturbations [22]. And the heat and particle deposition patterns on the divertor plate are closely related to the magnetic footprints, i.e. the strike points of open field lines with the divertor plates.

This work is devoted to study of the ELM crash caused by stochastic magnetic field on HL-2A tokamak, whose amplitude of precursor grows until a critical threshold to cause an ELM crash. The threshold indicates the magnetic perturbation may trigger the pedestal collapse and result in ELM crash. Nonlinear MHD simulations demonstrate that resistivity P-B modes are regarded as precursor mode and lead to magnetic reconnection at pedestal, which create magnetic island and then stochastic layer, resulting in the pedestal collapse. Furthermore, there is a threshold of magnetic perturbation to form stochastic layer with the geometry of the magnetic separatrix and X-point. The threshold indicates the sudden enhancement of transport and then leading to an ELM crash.

The paper is organized as follows. The experimental setup is displayed in section 2. In Section 3, numerical model of MHD simulation and a gyro-center particle code (GCP) is present. The experimental observations of ELM precursors on HL-2A tokamak are presented in section 4. Section 5 discusses the formation of stochastic layer, magnetic perturbation threshold of ELM crash. The conclusion and discussion are given in Section 6.

## 2. EXPERIMENTAL SETUP

HL-2A is a closed divertor tokamak with major radius R = 1.65 m and minor radius a = 0.4 m. The experiments discussed here are performed in a lower single-null (LSN) divertor configuration deuterium plasma with the H-mode discharge. The main discharge parameters are the following: the plasma currents Ip=150-170 kA in the anti-clockwise direction, the central chord-average electron density  $n_e = 1.5 - 2.5 \times 10^{19}$  m<sup>-3</sup>, and the toroidal field  $B_t = 1.3 - 1.4$  T in the clockwise direction. The auxiliary heating includes 700 kW of neutral beam injection (NBI) and 500 kW lower hybrid wave (LHW).

The line-averaged electron density was detected by using a far infrared interferometer-polarimeter [23]. A poloidal arrangement of 18 Mirnov coils at a minor radius of 50.5 cm is denoted using black solid points labelled by the numbers 1–18 in figure 1, and the sampling frequency is 1 MHz [24]. The magnetic fluctuations are measured by #13 poloidal Mirnov coil located in the outboard midplane. The divertor heat flux is calculated from the evolution of surface temperature on the target plates, measured by an IR camera [25][26]. Langmuir probe arrays with a spatial resolution of 6 mm are distributed in the region of  $Z = -0.755 \sim -0.875$  m on the outer divertor targets[27][28].

## 3. NUMERICAL MODEL OF ELM CRASH SIMULATION

The full set of resistive magnetohydrodynamic equations with CLT code is as follows[29][30]:

$$\frac{\partial \rho}{\partial t} = -\nabla \cdot (\rho \mathbf{v}) + \nabla \cdot [D\nabla(\rho - \rho_0)]$$

$$\frac{\partial p}{\partial t} = -\mathbf{v} \cdot \nabla p - \Gamma p \nabla \cdot \mathbf{v} + \nabla \cdot [\kappa \nabla (p - p_0)]$$

$$\frac{\partial \mathbf{v}}{\partial t} = -\mathbf{v} \cdot \nabla \mathbf{v} + (\mathbf{J} \times \mathbf{B} - \nabla p) / \rho + \nabla \cdot [\nu \nabla (\mathbf{v} - \mathbf{v}_0)]$$

$$\frac{\partial \mathbf{B}}{\partial t} = -\nabla \times \mathbf{E}$$

$$\mathbf{E} = -\mathbf{v} \times \mathbf{B} + \eta (\mathbf{J} - \mathbf{J}_0)$$

$$\mathbf{J} = \nabla \times \mathbf{B}$$
(1)

where  $\rho$ , p v, B, E, and J denote the plasma density, thermal pressure, plasma velocity, magnetic field, electric field, and current density, respectively. The subscript "0" denotes the equilibrium state. The term  $\eta J_0$  indicates Ohmic heating to sustain the plasma current.  $\Gamma$  (=5/3) represents the ratio of specific heat of plasma.  $\eta$ , D,  $\kappa$ , and  $\nu$  represent the resistivity, the plasma diffusion coefficient, the thermal conductivity, and the viscosity, respectively. The variables are normalized as follows:  $\mathbf{B}/B_{00} \to \mathbf{B}$ ,  $\mathbf{x}/a \to \mathbf{x}$ ,  $\rho/\rho_{00} \to \rho$ ,  $\mathbf{v}/\mathbf{v}_A \to \mathbf{v}$ ,  $t/\tau_A \to t$ ,  $\rho/(B_{00}^2/\mu_0) \to \rho$ ,  $J/(B_{00}/\mu_0 a) \to J$ ,  $E/(\mathbf{v}_A B_{00}) \to E$  and  $\eta/(\mu_0 a/\tau_A) \to \eta$ , where a is the minor radius, b00 and b00 are the initial magnetic field and the plasma density at the magnetic axis, respectively.  $\mathbf{v}_A = B_{00}/\sqrt{\mu_0 \rho_{00}}$  and  $\tau_A = a/\mathbf{v}_A$  are the Alfvén speed and Alfvén time at the magnetic axis.

In order to study the heat flux loss during ELM crash, a gyro-center particle code has been developed. In the guiding-center phase space  $(X, v_{II})$ , where X represents the guiding-center position and  $v_{II} = \mathbf{b} \cdot \dot{X}$  denotes the guiding-center parallel velocity, they will be described by [31] [31]

$$\frac{d\mathbf{X}}{dt} = \frac{1}{B_{//}^*} \left( v_{//} \mathbf{B}^* + \mathbf{E}^* \times \mathbf{b} \right)$$

$$\frac{dv_{//}}{dt} = \frac{Z\mathbf{e}}{\mathbf{m}B_{//}^*} \mathbf{B}^* \cdot \mathbf{E}^*$$
(2)

Where  $B^*_{//} = \mathbf{b} \cdot \mathbf{B}$ , (**b** is the unit vector of the magnetic field), is the effective magnetic field  $\mathbf{B}^*$  in the parallel direction. The electromagnetic fields associated with the stochastic field are derived from the CLT code. In our simulations, during the ELM crash, we assumed that the heat flux is contributed solely by deuterium ions starting from the stochastic layer and ending with striking on the divertor. The heat load at diverter region is described by

$$q(X) = \int E f dv^3 = \sum_{i=1}^n \frac{1}{2} m v_i^2 \delta(X - X_i)$$
(3)

where f and E represent the ion distribution function and energy. And m,  $v_i$  and  $X_i$  are the test particle mass, velocity and position. It is important to note that only the particles striking on the divertor plate  $(X_i = X)$  are counted. In the orbit step, the fourth-order Runge–Kutta algorithm is employed. Both the step size and grid number will influence the accuracy. A uniform mesh of size  $256 \times 64 \times 256$   $(R, \phi, Z)$  is utilized for both MHD and particle simulations, with a resolution of  $\Delta R = 0.0036m$ ,  $\Delta \phi = \pi/32$ , and  $\Delta Z = 0.0041m$ . The time advancement of the particle part is the same as that of MHD part. The time step dt is calculated in MHD part to satisfy the Courant–Friedrichs–Lewy (CFL) condition in whole simulation domain. And explicit scheme is used for time advancing. Therefore, the dt is rather small, which completely satisfies the convergency of particle simulation. But the time consumption also becomes huge because of a large number of particles tracing. Combination of CUDA and MPI technologies on multiple GPUs, the CUDA heterogeneous parallel programming model is successfully applied to acceleration of the particle tracing code.

## 4. EXPERIMENTAL OBSERVATIONS OF ELM PRECURSOR

The typical ELM intervals are 1–3 ms with some exceptions of more than 10 ms on HL-2A [20][32]. Distinct precursor modes associated with ELM crashes, are often observed by Mirnov coils in HL-2A H-mode plasmas. In shot 34543, the toroidal magnetic field is  $B\sim1.35$  T, the plasma current is 150 kA, the line-averaged plasma density is  $(1.5-2.8)\times10^{19}$  m<sup>-3</sup>. The heating powers of NBI and LHW are about 0.7 MW and 0.5 MW, respectively. A zoom-in example for the precursor modes in shot 34543 is shown in figure 1. An ELM crash is demonstrated by the burst of D $\alpha$  signal, as shown in figure 1(a). The ELM precursor is identified from the Mirnov signal in figure 1(b). The precursor starts to grow for 6~7 ms before the onset of an ELM, which can be shown the time trace of magnetic perturbations measured in 972-978 ms or 979-985 ms. The ELM precursor with frequency  $f\sim15$  kHz lasts  $\sim6$  ms in figure 1(c). Figure 1(d) shows the amplitude of ELM precursor mode for a few milliseconds

after/before the ELM event. The amplitude grows till a critical threshold to trigger an ELM crash. Result indicates that ELM crash seems to be terminated by the coherent magnetic perturbation. Moreover, the amplitude of ELM precursor does not grow exponentially into the ELM crash but mostly rather linearly towards  $\delta B_C$ . Therefore, this should not be explained by explosive instability.

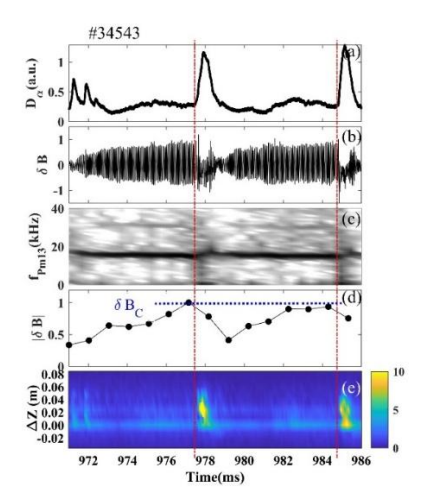


Figure 1. The zoom-in time trace of precursor perturbations measured in 972~986 ms. Da emission (a), Mirnov signal (b), its frequency spectrum (c) and amplitude (d), and the distribution of the saturation ion current density on the outer divertor target (e).

## 5. SELF-CONSISTENT SIMULATION OF ELM CRASH

To gain insight into a threshold of magnetic perturbation as the mechanism to trigger ELM crash in the H-mode regime, extensive numerical simulations have been performed. This work is carried out by using CLT code [29][30]. We choose a lower single-null divertor configuration of HL-2A plasma equilibria generated by the CLT-EQ module, which consists of the X-point, the separatrix, and the scrape-off layer (SOL)[33]. This model equilibria will be simulated for H-mode plasmas with steep pressure and current at the edge. In the present model, equilibrium flow has been set to be zero. The parameters are chosen to be  $\eta=1.0\times10^{-6}$ ,  $D=1.0\times10^{-6}$ ,  $L=1.0\times10^{-6}$ ,  $L=1.0\times10^{-6}$ ,  $L=1.0\times10^{-6}$ , and  $L=1.0\times10^{-6}$ , A uniform mesh of size  $L=1.0\times10^{-6}$ ,  $L=1.0\times10^{-6}$ , and  $L=1.0\times10^{-6}$ , are further parallelized using NVIDIA GPUs[34].

In the linear phase, the mode grows exponentially from the noise level with a linear growth rate of 0.0692  $\tau^{-1}_A$ . The pressure and current free energies drive the MHD instability (namely P-B modes) and produce the radial magnetic field ( $\delta B_r$ ). The latter creates the magnetic islands. And we find that a stochastic magnetic field is generated when the amplitude of  $\delta B_r$  reaches a threshold, which greatly enhance the transport and lead to ELM crash. In the nonlinear simulation, field line tracing indicates the creation of magnetic islands and stochastic magnetic field during resistive P-B modes, as shown in figure 2. The stochastic layer suggests that the particles losses, along parallel to magnetic fields, can be significant. Specifically, the non-axisymmetric of magnetic perturbation  $(\delta B_r)$ , derived from steep pressure and current, may create the magnetic islands and change the magnetic configuration, as shown in figure 2(b, c). When the amplitude of  $\delta B_r$  reaches the threshold, an edge stochastic magnetic field is generated, as shown in figure 2(d). The edge stochastic layer greatly enhances radial particle transport along magnetic field lines, which results in collapse of the pedestal pressure and ELM crash. In this crash process, the free energy of P-B modes is rapidly released, which suddenly decreases the pressure gradient or current. After the crash, the P-B instability becomes rather weak. And the low magnetic perturbation allows the good magnetic topology and confinement. Afterwards, this pressure or current profile are slowly recovered to a steep profile through heating and fuelling. The new sharp profiles may provide the conditions for the next ELM crash.

#### **AUTHOR and OTHER-AUTHOR**

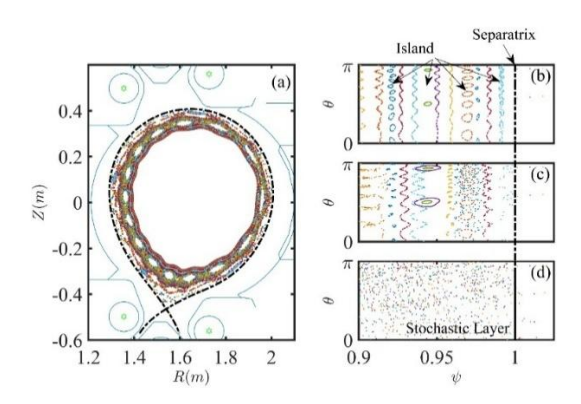


Figure 2. Poincare plots of the magnetic field with resistive P-B modes in the HL-2A poloidal section (a), and a zoom-in configuration view of boundary region  $\psi = [0.9 \ 1.025]$  in PEST coordinate at time slices 383  $\tau A$  (b), 400  $\tau A$  (c), and 487  $\tau A$  (d).

In this simulation, we find that the resistivity P-B modes dominate the magnetic reconnection on the pedestal region. The perturbed magnetic ( $\delta B_r$ ), driven by P-B instability, creates the chain of magnetic island in plasma edge. The width of magnetic island ( $w_{mn}$ ) can be calculated as [35] [36][37],

$$w_{mn} = \sqrt{\frac{16}{m} \frac{q}{q'} \frac{S}{(2\pi)^2} B_{m,n}^r}$$
 (4)

where  $q = dq/d\psi$  (q is the safety factor). S is the surface area at the rational surface. The well-known Chirikov criterion for stochasticity or island overlapping condition in magnetically confined plasma can be written as [38],

$$\sigma_{12} = \frac{w_{m1,n1} + w_{m2,n2}}{2|\rho_2 - \rho_1|} \ge 1 \tag{5}$$

where  $\sigma_{12}$  is the Chirikov parameter determined by the two adjacent islands located at  $\rho_1$  and  $\rho_2$ , respectively. The magnetic island is formed when the radial magnetic perturbation ( $B^r_{mn}$ ) is large enough on its rational surface. The island width of each harmonic (m, n) can be evaluated from the spectrum of the radial magnetic perturbation derived by P-B mode instability. In our simulation, the P-B mode instability is obtained from CLT code. Figure 3 shows that the time evolutions of the island width located at flux surface  $\sqrt{\psi} = 0.83, 0.88, 0.95, 0.97, 0.98, 0.99$ .

As the development of P-B instability, the perturbations of radial magnetic field may make the magnetic islands overlap. The distance between separatrix ( $\psi$ =1) and the innermost surface where the islands are overlapped is used as a figure of merit for the stochastic field level. The stochastic layer forms with enough large magnetic island or amplitudes of magnetic perturbation.

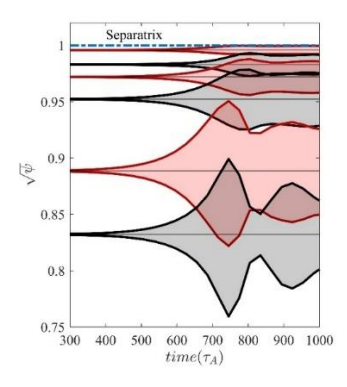


Figure 3. The time evolutions of the island width located at flux surface  $\sqrt{\psi}$  =0.99, 0.98, 0.97, 0.95, 0.88, 0.83.

In the flux coordinates  $(\psi, \theta, \zeta)$ , the magnetic field in a tokamak can be written as  $\mathbf{B} = \nabla \psi_t \times \nabla \theta - \nabla \psi \times \nabla \zeta$ , where  $\psi_t$  and  $\psi$  are the toroidal and poloidal magnetic flux.  $\theta$  and  $\zeta$  are the poloidal and toroidal angles. We label poloidal flux  $\psi$  as the Hamiltonian  $H(=\psi)$ . The system is governed by the following Hamiltonian [39][40]

$$\frac{d\psi_{t}}{d\xi} = -\frac{\partial H}{\partial \theta} \quad \frac{d\theta}{d\xi} = \frac{\partial H}{\partial \psi_{t}} \tag{6}$$

In this formalism,  $(\psi_t, \theta)$  appear as a pair of canonical variables. The Hamiltonian of the system is  $H = H_0(\psi_t) + H_1(\psi_t, \theta, \zeta)$ , which can be expressed as a sum of the unperturbed flux  $H_0(\psi_t)$  and of the perturbation

$$H_1(\psi_t, \theta, \zeta) = \sum_{m,n} H_{mn}(\psi_t) \cos(m\theta - n\zeta + \chi_{mn})$$
(7)

where  $H_{mn}(\psi_t)$  is the Fourier coefficient of the perturbed poloidal flux, and  $m\theta - n\zeta + \chi_{mn}$  is the helical angle of the m/n harmonic perturbation. The presence of a resonant perturbation may produce many small islands. If the islands are separated by quite a large distance, they do not overlap for the small perturbation amplitudes, as shown in figures 2(b). If they are locked together, they generate a weak chaotic regime, implying the chaotic zones surrounding the islands, as shown in figures 2(c). However, for large perturbation amplitudes the islands will overlap producing a large chaotic zone (or stochastic layer) around them, as shown in figure 2(d). Stochastic layer is important in determining the particle guiding center orbit, the plasma stability, and the transport process.

To study the influence of the magnetic perturbation on stochastic layer, connection length  $(L_{\rm C})$  is defined as the turn number of toroidal rotation of one field line from the initial point in plasma to the striking point on the divertor or exceeding a specific maximum toroidal turn [41].  $L_{\rm C}$  is used as the stochastic level of the layer. The guiding-center particles will escape from the plasma region along magnetic field line, if the field line strikes the diverter. The escape time is  $\tau_{\rm C}=2\pi R_0 L_{\rm C}/C_{\rm s}$ , where the  $C_{\rm s}=\sqrt{(T_i+T_e)/m_d}$  is the ion acoustic velocity,  $T_{\rm i}$  and  $T_{\rm e}$  are the ion and

electron temperature,  $m_d$  is the mass of deuterium ions, and  $R_0$  is major radius. This  $\tau_C$  will serve as the rise time  $(\tau_{rise})$  of ELMs energy pulse to the divertor target. The ELM energy pulse to the divertor target can be divided into two phases (the rise stage and the decay stage). The characteristic timescale  $\tau_{rise}$  for the first phase is defined as the duration of the power increase from 10% above the initial value to 100% of the maximum measured value, and the decay time  $\tau_{decay}$  for the second phase is the duration from the peak power to 1/e decay[42]. The power rise and decay times of a total of 80 ELM crash events are plotted. The observed rise times are between about 200 μs to 500 μs with an average of 332 μs, and the decay times are typically 300 to 700 μs with an average of 415 μs, longer than the corresponding rise times. Assuming  $T_{\rm i} = T_{\rm e} = T_{\rm ped}$ ,  $T_{\rm ped}$  is the pedestal values of ions temperature. On HL-2A, pedestal temperature is about  $T_{\rm ped} \approx 0.2$  keV and  $\tau_{\rm rise} \approx 332$  µs, resulting in an ion acoustic velocity  $C_s \approx 140$  km/s and a connection length of about  $L_C = C_s \tau_{rise}/(2\pi R_0) \approx 4.4$  (turns). Figure 4 shows the edge connection length against the perturbation amplitudes in the HL-2A divertor configuration. The magnetic lines will strike on the divertor, if  $L_C < 10$  (escape lines, the corresponding escape times  $\tau_C = 2\pi R_0 L_C / C_s \approx 750 \,\mu s \sim \tau_{rise}$ ). The magnetic lines will keep within the separatrix, if their connection length reaches 1000 turns (confined lines, the corresponding escape times  $\tau_C \approx 75000 \,\mu s \gg \tau_{rise}$ ). In figure 4, a threshold of magnetic perturbation  $\delta B_C$  is found, indicating that the magnetic field lines remain within the separatrix if  $\delta B < \delta B_C$ . And the particles are well confined inner the separatrix. If the  $\delta B > \delta B_C$ , the field lines turn into stochastic. The magnetic field line connects to divertor plates, resulting in particles transiently dumping energy into the SOL. The threshold of magnetic perturbation  $\delta B_{\rm C}$ likes a magnetic trigger for causing transient energy loss. This is consistent with the experimental observation, the amplitude of precursor gradually growing till a critical threshold, to cause an ELM crash, as shown in figure 1.

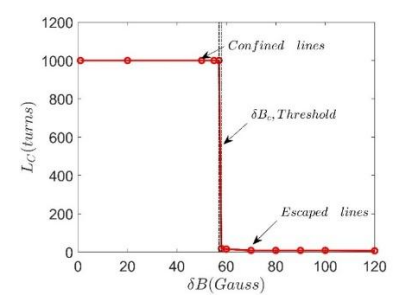


Figure 4. Connection length or turn number of toroidal rotation (Lc) of the field lines against different perturbation amplitudes ( $\delta B$ ) at X point.

#### **AUTHOR and OTHER-AUTHOR**

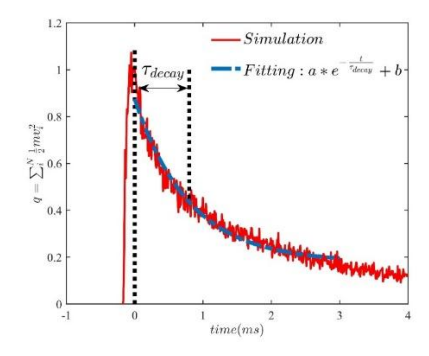


Figure 5. The simulation temporal evolution of ELM crash event with stochastic field. The decay time is estimated about 800 µs, which is consistent with experimental statistics.

In order to study the heat flux loss during an ELM crash, a code of gyro-center particles has been developed. A number of test particles (>10<sup>5</sup>) are initially distributed at the stochastic region, where particles may lose during ELM crash. Initial velocity of particles is determined by Maxwellian distribution. After the initialization, their guiding-center motions are solved by formula (2) using fourth-order Runge-Kutta algorithm. Particles starting from the stochastic region to the striking points on the divertor plates are counted. Their heat flux is described by formula (3). Figure 5 shows the simulation temporal evolution of heat flux in divertor during an ELM crash event with stochastic field. The simulated decay time is estimated about 700  $\mu$ s, which is consistent with the experiment statistics decay times ( $\tau_{decay}$  =300~700  $\mu$ s).

## 6. CONCLUSION AND DISCUSSION

In the present work, we find a threshold of magnetic perturbation to trigger ELM crash. The ELM precursor is identified from the Mirnov signal for  $6\sim7$  ms with frequency  $f\sim15$  kHz before an ELM crash. The amplitude of precursor grows until a critical threshold to cause an ELM crash. The precursor threshold indicates that the magnetic perturbation triggers the pedestal collapse and results in ELMs crash. Nonlinear MHD simulations demonstrate that stochastic layer is generated by magnetic reconnections process of resistivity P-B modes. The non-axisymmetric magnetic perturbation, derived from P-B modes, creates the magnetic islands and then stochastic layer. The formation of edge stochastic magnetic field greatly enhances radial particle transport along magnetic field lines, which results in collapse of the pedestal pressure and an ELM crash. Furthermore, there is also a threshold of magnetic perturbation leading in  $L_{\rm C}$  changes, which responds for the sudden ELM crash. These results clearly prove that ELM crash is triggered by stochastic field with a threshold of magnetic perturbation.

## 7. REFERENCES

- [1] Valentin Igochine, Springer Berlin Heidelberg, 2015
- [2] ITER Physics Expert Group on Divertor, Nucl. Fusion, 39(1999), 2391
- [3] A Loarte et al. Plasma Phys. Control. Fusion, 44(2002), 1815
- [4] A. Zhitlukhin et al. J. Nucl. Mater. 363-365 (2007), 301-307
- [5] T. Ozeki, et al. Nucl. Fusion, 30(1990), 1425
- [6] Y Kamada et al. Plasma Phys. Control. Fusion, 42(2000), A247
- [7] Y Kamada et al., Plasma Phys. Control. Fusion, 44(2002), A279
- [8] G. S. Xu *et al.* Phys. Rev. Lett. 122(2019), 255001
- [9] R. Maingi *et al*. J. Nucl. Mater. 337–339(2005), 727–731
- [10] HR Wilson et al. Plasma Phys. Control. Fusion, 48 (2006), A71-A87
- [11] P. B. Snyder et al. Physics of Plasmas, 9 (2002), 2037

# [Right hand page running head is the paper number in Times New Roman 8 point bold capitals, centred]

- [12] Steven C Cowley et al. Control. Fusion, 45(2003), A31–A38
- [13] H. R. Wilson et al. Phys. Rev. Lett. 92(2004), 175006
- [14] S. C. Cowley et al. Proc. R. Soc. A, 471: 20140913(2015)
- [15] F M Poli et al. Plasma Phys. Control. Fusion, 50(2008), 095009
- [16] C.P. Perez et al. Nucl. Fusion, 44(2004), 609-623
- [17] H.R. Koslowski et al. Nucl. Fusion, 45(2005), 201–208
- [18] A L Colton et al. Plasma Phys. Control. Fusion, 38(1996), 1359
- [19] W Suttrop et al. Plasma Phys. Control. Fusion, 38(1996), 1407
- [20] Y. Huang et al. Nucl. Fusion, 52(2012), 114008
- [21] X. Q. Xu et al. Phys. Rev. Lett. 105(2010), 175005
- [22] S. S. Abdullaev, Nucl. Fusion, 54(2014), 064004
- [23] Y. Zhou et al. Rev. Sci. Instrum.,83(2012), 10E336
- [24] JI Xiao Quan et al. Chin. Phys. Lett. 27(2010), 065202
- [25] Gao J M et al. Chin. Phys. B 22(2013), 015202
- [26] J.M. Gao et al. Nucl. Fusion, 61 (2021), 066024
- [27] Zhihui HUANG et al. Fusion Sci. Technol. 24 (2022), 054002
- [28] N Wu, J Cheng et al. Plasma Phys. Control. Fusion, 63(2021), 075002
- [29] S. Wang and Z. W. Ma, Physics of Plasmas, 22(2015), 122504.
- [30] W. Zhang et al. Computer Physics Communications, 228(2021), 44–53
- [31] John R. Cary and Alain J. Brizard, Rev. Mod. Phys. 81(2009), 693
- [32] Huang Yuan et al. Chin. Phys. B, 20(2011), 055201
- [33] W. J. Chen et al. Plasma Science and Technology, 24, 035101(2022).
- [34] H. W. Zhang et al. Int. J. Comput. Fluid Dynam. 33 (2019), 393
- [35] Y Sun et al. Plasma Phys. Control. Fusion 57 (2015) 045003
- [36] Bécoulet M et al. Nucl. Fusion, 48(2008), 024003
- [37] M.J. Schaffer et al. Nucl. Fusion 48(2008), 024004
- [38] Chirikov B.V. 1979 A universal instability of many-dimensional oscillator systems Phys. Rep.52 263-379
- [39] D. Constantinescu et al. Nucl. Fusion, 48(2008), 024017
- [40] Allen H. Boozer, Rev. Mod. Phys., 76(2005),1071-1141
- [41] M Jia et al. Plasma Phys. Control. Fusion 58(2016), 055010
- [42] J.M. Gao et al. Nucl. Fusion 61(2021), 066024